Journal of Materials Chemistry A

Revealing cooperative Li-ion migration in Li1+xAlxTi2-x(PO4)3 solid state electrolyte with high Al doping

Journal:	*Journal of Materials Chemistry A*
Manuscript ID	TA-ART-09-2019-009770.R2
Article Type:	Paper
Date Submitted by the Author:	20-Nov-2019
Complete List of Authors:	Zhang, Bingkai; Peking University, School of Advanced Materials Lin, Zhan; Guangdong University of Technology, School of Chemical Engineering and Light Industry Dong, Huafeng; Guangdong University of Technology, School of Physics and Optoelectronic Engineering Wang, Lin-Wang; Lawrence Berkeley National Laboratory, Pan, Feng; Peking University, School of Advanced Materials

Revealing cooperative Li-ion migration in $Li_{1+x}Al_xTi_{2-x}(PO_4)_3$ solid state electrolyte with high Al doping

Received 00th January 20xx,
Accepted 00th January 20xx

DOI: 10.1039/x0xx00000x

Bingkai Zhang,[a,b] Zhan Lin,[a] Huafeng Dong,[c] Lin-Wang Wang,[d*] and Feng Pan[b*]

$Li_{1+x}Al_xTi_{2-x}(PO_4)_3$ (LATP) is attracting attention as a promising inorganic solid electrolyte (ISE) with potential use in all-solid-state lithium-ion batteries. The objective of this paper is to examine and understand the effect of the Al-dopant concentration on the Li-ion diffusion of LATP using density functional theory and molecular dynamics method. By comparing $Li_{1.16}Al_{0.16}Ti_{1.84}(PO_4)_3$ (LATP-0.16) and $Li_{1.33}Al_{0.33}Ti_{1.67}(PO_4)_3$ (LATP-0.33) with $Li_{1.5}Al_{0.5}Ti_{1.5}(PO_4)_3$ (LATP-0.50), LATP-0.50 is expected to have higher ionic conductivity. The trapping effect of Al-dopants on Li-ions is greatly reduced in LATP-0.50 due to the delocalization of polarization interactions and the depopulation of oxygen atoms, which results in a smooth energy landscape and destabilization of Li-ions. The energy difference of adjacent Li-ions and binding interaction of Li-Li due to specific local two Li-ions' configuration alternately enable Li-ions' cooperative migration. This understanding of high Li-ion diffusion is important in interpreting experimental results aiming to assess the effects of Al-dopant in Li-ion conductivity and can be used by researchers to engineer this material for batteries.

Introduction

All-solid-state lithium batteries (ASSLBs) have been extensively studied due to their stability to lithium metal anode and high safety.[1-4] One of the most important challenges in ASSLBs is to design solid electrolytes with high ionic conductivity.[5-7] Right now, the use of inorganic solid electrolytes (ISEs) is a field of continuous interest in ASSLBs,[8-11] but the optimum compound is yet to be found. In terms of ionic conductivity, only a few ISEs have been considered on par with those of liquid electrolytes.[1,3] One approach for further improvement is to understand and fine-tune the already discovered fast Li-ion solid conductors such as the Al-doped $LiTi_2(PO_4)_3$ (LTP) named as $Li_{1+x}Al_xTi_{2-x}(PO_4)_3$ (LATP). The improvements in these materials can boost the properties of ISEs to a new level.[12]

Interstitial Li-ions created by the substitution of aliovalent Al^{3+} cations have been considered the sources of ionic conductivity in LATP, and as a consequence, the ionic conductivity may increase with the concentration of interstitial Li-ions as some experiments have proved.[13-18] However, current experiments concentrates more attention on $Li_{1.2}Al_{0.2}Ti_{1.8}(PO_4)_3$ (LATP-0.20) or $Li_{1.3}Al_{0.3}Ti_{1.7}(PO_4)_3$ (LATP-0.30) rather than the $Li_{1.5}Al_{0.5}Ti_{1.5}(PO_4)_3$ (LATP-0.50) with higher Al-dopants.[17,19,20] To date, there is no general agreement on the optimum Al-dopants in LATP.

Furthermore, interstitial migration in LATP, in particular, has a low barrier to enable high ionic conductivity.[21,22] Nevertheless, the structural and chemical origin of the interstitial migration is not understood, preventing the rational design of better ISEs. The well-defined atomistic structure of LATP provides us an ideal model system to probe the interstitial migration mechanism.

In this work, we chose to study three LATP systems with different compositions: $Li_{1.16}Al_{0.16}Ti_{1.84}(PO_4)_3$ (LATP-0.16), $Li_{1.33}Al_{0.33}Ti_{1.67}(PO_4)_3$ (LATP-0.33) and $Li_{1.5}Al_{0.5}Ti_{1.5}(PO_4)_3$ (LATP-0.50), along with LTP as a reference, to understand the ionic conductivity of LATP. Most researches so far find when Al content above 0.5, additional phosphate phases appear in LATP that slows down diffusion.[14,17,23,24] Therefore, in this work, we combine density functional theory (DFT) and *ab-initio* molecular dynamics (AIMD) simulation techniques to probe Li-ion migration mechanism in the LATP ($0.0 \le x \le 0.5$). In particular, the results obtained from DFT and long time-scale AIMD provide new insights into the mechanistic features of Al-dopants and lithium-ion (Li-ion) transport. These techniques have been applied successfully to a variety of studies on ionic or mixed conductors.[12,25-28]

Results and discussion

Structural modeling

The LTP crystal structure has hexagonal symmetry and is composed of corner-sharing TiO_6-PO_4 units (Fig. 1a).[29-31] Distribution of Li-ions in Li(1) (6b), Li(2) (18e) and Li(3) (36f) positions is shown in right inset of Fig. 1a. The Li(1) site is

[a] School of Chemical Engineering and Light Industry, Guangdong University of Technology, Guangzhou 510006, China
[b] School of Advanced Materials, Peking University, Shenzhen, China. E-mail: panfeng@pkusz.edu.cn.
[c] School of Chemical Engineering and Light Industry, Guangdong University of Technology, Guangzhou 510006, China
[d] School of Physics and Optoelectronic Engineering, Guangdong University of Technology, Guangzhou 510006, China.
[e] Materials Sciences Division, Lawrence Berkeley National Laboratory, Berkeley, CA 94720, United States. E-mail: lwwang@lbl.gov
Electronic Supplementary Information (ESI) available: [details of any supplementary information available should be included here]. See DOI: 10.1039/x0xx00000x

located in the LiO_6 octahedrons, Li(2) site is at each bend of the conduction channels, and Li(3) site is adjacent to Li(1) site along conduction channel. The Li-ion diffusion pathway performed by the bond-valence method (analysis of valence mismatches)[32] is zigzag-shaped channel along the c-axis is shown in Fig. 1b. Li-ion migration within this system is restricted to within the channels of corner-sharing PO_4 tetrahedral and TiO_6 octahedral.

To model LATP-0.16, LATP-0.33 and LATP-0.50, one, two, and three Ti atoms from the original twelve sites are replaced by Al atoms, respectively. The substitution of each Ti^{4+} by Al^{3+} needs an extra Li-ion for charge compensation and these Li-ions can occupy in either Li(2) or Li(3) sites. To check the stability of extra Li-ion at these two sites, the optimized local configuration of LATP-0.16 is calculated as shown in Fig. 1c. For the case of extra Li-ion occupying Li(3) site, the interaction and steric effects between neighboring Li(1) and Li(3) positions leads to the displacement of Li(1)-ion and thus form two Li(3)-ions. For the case of extra Li-ion occupying Li(2) site, the positions of neighboring Li(1)-ions are slightly displaced. The configuration energies of these two cases are nearly the same, suggesting these configurations coexist in real experiments. In addition, Al-dopants in the LATP tend to have a dispersed distribution rather than agglomeration according to the calculated configuration energy shown in Fig. S1 of ESI.

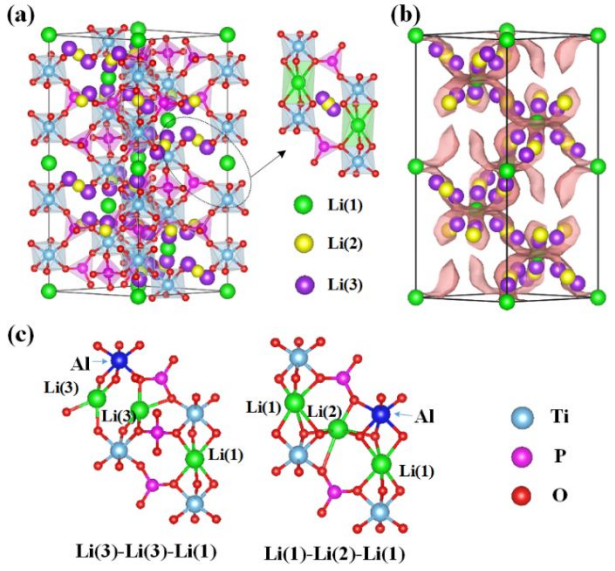

Fig. 1. (a) Polyhedral representation of the crystal structure of LTP and visualization of local structure for Li-ion migration (right inset). (b) The potential diffusion pathway illustrated by the Bond-valence mismatch method, and visualization of three Li-ions' positions: M1 (6b), M2 (18e) and M3 (36f). (c) Local structure for LATP-0.16 with two Li-ions configurations.

To study the influence of Al-doping concentration on the stability of Al-dopants in LATP, we calculate the Al defect formation energy (Al-DFE) in LATP and phase decomposition energy (PDE) of LATP (detailed in the ESI). The results suggest that the Al defect formation energies in LATP-0.33 (2.98 eV) and LATP-0.50 (3.10 eV) are very close. The decomposition energies for LATP-0.16, LATP-0.33 and LATP-0.50 are 262.41, 389.93, and 642.34 meV/atom, respectively. A positive value of Al-DFE or PDE signifies the unfavorably thermodynamic reaction. We note that the extent of Al defect formation and phase decomposition for LATP-0.33 is even a little higher than that for LATP-0.50. Now many experiments have successfully demonstrated the synthesis of LATP-0.50.[17] Thus, the stability of Al-dopant in LATP-0.50 is less problematic in practice because the thermodynamically unfavorable reactions and associated kinetic barrier.

Statistics of Li-ion hopping in LTP and LATP

To visualize the Li-ion diffusion paths and probe transport mechanism, we perform the lithium dynamic diffusion using AIMD method on six LTP or LATP units. Fig. 2a, 2b, 2c, and 2d show trajectory plots of Li-ion positions for LTP, LATP-0.16, LATP-0.33, and LATP-0.50 from an AIMD run (500 K), respectively. Fig. 2a clearly indicates small vibrations of Li-ions around their lattice sites, demonstrating a typical behavior of an ordered crystalline solid with no evidence of ion diffusion. This result suggests that Li-ion dynamics in LTP is a local oscillation. Comparing the shape and size of the spatial densities of the Li-ions obtained from the trajectory plots with those of the thermal ellipsoids from the neutron diffraction experiment[33], we see a very good agreement.

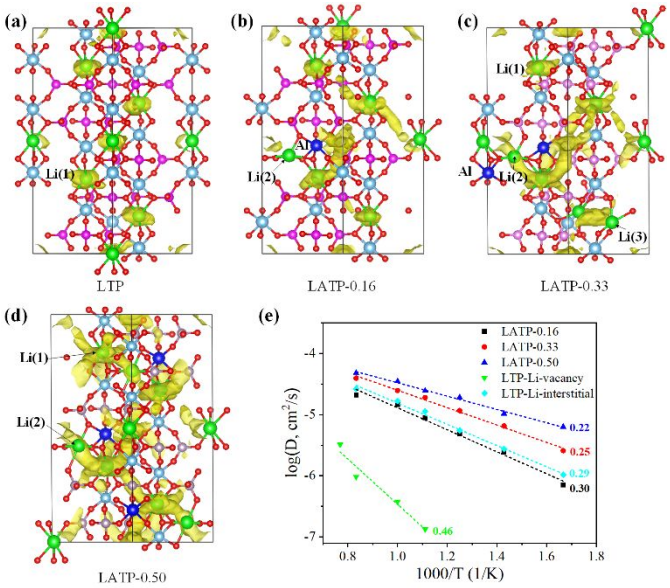

Fig. 2. (a), (b), (c) and (d) The trajectory density (1×10^{-3} Å^{-3} isosurface level) of Li-ions in LTP, LATP-0.16, LATP-0.33 and LATP-0.50 taken from 80 ps NVT AIMD simulations at 500 K. (e) Effect of Al-doping and carrier (Li-vacancy and Li-interstitial) on diffusivity in the LTP structure. The corresponding activation energies (in eV) are given. Data points at 600 K, 700 K, 800 K, 900 K, 1000 K and 1100 K in the AIMD simulations.

When two Al-Li pairs are present in LTP, i.e., LATP-0.33, there is some movement of the Li-ions (Fig. 2c). The diffuse distribution and overlapping of different Li positions indicate that Li-ions are moving through the interstitial sites, suggesting an interstitial mechanism. With the increasing of Al-dopants (i.e., LATP-0.50 of Fig. 2c), all of the Li-ions are involved in the diffusion of lithium. To prove the effective jump of Li-ion in LATP, we calculate the site displacement function (SDF) plots for Li-ion trajectories (Fig. S2 in ESI) in LATP-0.50 taken from 80 ps NVT

AIMD simulations at 600 K. The SDF result suggest the migration distance of Li-ion is more than 9 Å.

The calculated diffusivity and activation energy of LATP is present in Fig. 2e. We find that Al-doping enhances Li-ion conductivity. The increase in Li conductivity is consistent with the experimental observations that ISEs with high Li-ion content tend to be better Li-ion conductors. The calculated activation energy for LTP (Li-ion migration via vacancy), LATP-0.16, LATP-0.33 and LATP-0.50 is 0.46, 0.30, 0.25, and 0.22 eV, respectively. In addition, we also calculate the interstitial migration by adding one interstitial Li-ion in LTP (with six LTP units). The calculated migration barrier is about 0.29 eV, suggesting interstitial migration is more favourable than vacancy migration. Our results agree with the previous experiments that suggest LATP-0.50 has high Li-ion diffusivity.[13,14,34] The activation energy of LATP-0.50 is also in agreement with that obtained by lithium nuclear magnetic resonance (NMR) spectroscopy experiment (0.16-0.17 eV).[13] The activation energy of LATP-0.50 is significantly lower than that of garnet-type $Li_7La_3Zr_2O_{12}$ (LLZO) (0.34 eV)[35] and is close to that of $Li_{10}MP_2S_{12}$ (M = Ge, Si, or Sn) group (0.18-0.20 eV)[36]. Therefore, the Li-ion diffusivity in LATP-0.50 is among the best in known solid electrolytes, and the related mechanism is interested to get insight by analysis of structure evolution during the Li-diffusion.

Valuable structural information can be revealed from radial distribution functions (RDFs), which often provide insight into the long-range (dis)order of the material. Fig. 3 shows the RDFs for Li-Li and partial RDFs for O-Li calculated over the simulation time. There are three important features. First, with the increase of Al-dopant, the distance of Li-Li pair (e.g. Li(1)-Li(1), Li(3)-Li(3)) is reduced and the amplitude of Li(3)-Li(3) peak is higher than those of Li(1)-Li(1) (Fig. 3a). Second, Li-ions originally in Li(3) sites are more mobile as demonstrated by the lack of structure beyond the first coordination shell (Fig. 3b), indicative of the greater disorder. Third, the partial RDFs peaks for O-Li(1) and O-Li(3) in LATP-0.50 (Fig. 3c) are almost same, indicating faster Li-ion mobility happens, thus difficult to distinguish Li(3) and Li(1), which reveals the feature of cooperative Li-ion migration cooperation.

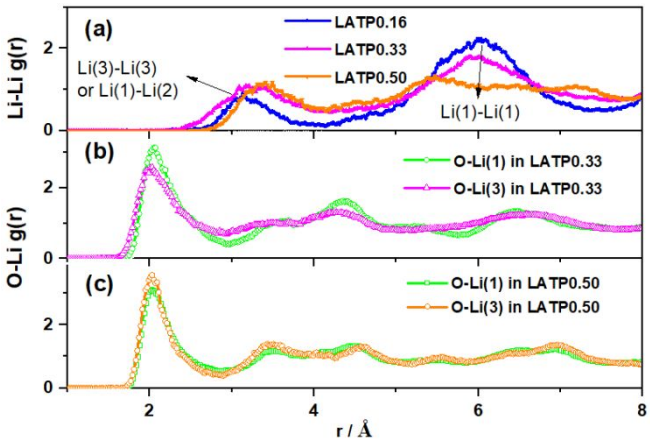

Fig. 3. RDFs for Li-Li interactions in LATP-0.16, LATP-0.33 and LATP-0.50 from NVT (600 K, 80 ps) AIMD simulations. Two sharp peaks located at 3.3 Å and 6.0 Å are for Li(1)-Li(1) Li(3)-Li(3) in LATP, respectively. (b) and (c) Partial RDFs for O-Li interactions in LATP-0.33 and LATP-0.50 from NVT (600 K, 80 ps) AIMD simulations.

To further examine the Al-doping effect on Li conduction, statistical analysis of Li diffusion is performed by calculating the Li-Li space-time correlation functions[37] for LATP-0.16 and LATP-0.50, as shown in Fig. 4. The detailed introductions of the space-time correlation functions are shown in the SI. The defined $G_s(r, t)$ gives the probability that, at time t, an atom will be located a position that has a distance (r) from another location which is occupied by another atom at time zero. For LATP-0.16, in Fig. 4a, the $G_s(r, t)$ plots show one peak appearing between 0 and 2.5 Å with weak time dependence, suggesting atomic vibrations around equilibrium positions. For LATP-0.50, in Fig. 4c $G_s(r, t)$ curves have a much weaker intensity of peaks, indicating a lower probability of finding a Li-ion around its original position and showing a faster Li-ions mobility in LATP-0.50.

The defined $G_d(r, t)$ (right insets of Fig. 4) gives the probability of finding Li-ion j at distance r after a time interval of t, in relation to the position of another Li-ion i at the initial time t = 0. When t = 0, $G_d(r,t)$ is collapsed to the $g(r)$ function of Li–Li. In the cooperative migration, $r_j(t) - r_i(t = 0)$ progressively approaches zero with time and causes the $G_d(r, t)$ contribution near r = 0 to increase rapidly. Actually, we can identify a characteristic time t_{max} above which the level of $G_d(r, t)$ does not increase anymore, or it starts decreasing. This time scale can be taken as a measure for the average time required in order that a Li-ion is knocked-off with a different one; that is, a cooperative migration between Li-ions has been realized. For LATP-0.16 (Fig. 4d), t_{max} is estimated close to 21 ps; for the LATP-0.50 (Fig. 4d), close to 12 ps. Comparing these time scales, it appears that the latter is shorter, as expected due to their cooperative nature. Therefore, high content Al-doping in the NASICON structure may modify the potential energy surface of Li-ions, which allows considerable Li-ions hopping to occur between lattice sites.

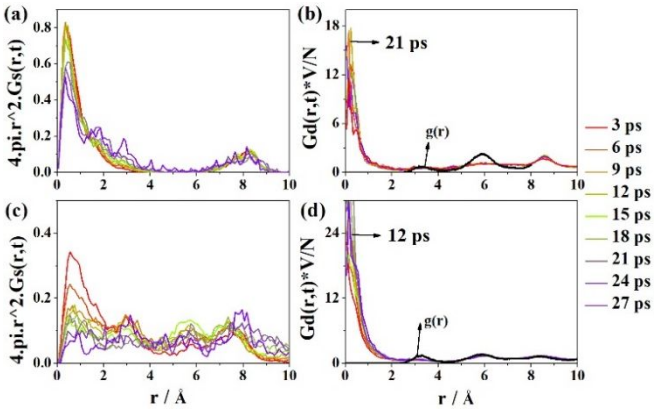

Fig. 4. (a) and (b) $G_s(r, t)$ and $G_d(r, t)$ of the van Hove correlation function for the Li motion (3-27 ps) from NVT MD simulation at 900 K in LATP-0.16. (c) and (d) $G_s(r, t)$ and $G_d(r, t)$ functions for Li-ion motion in LATP-0.50.

In addition, to evaluate whether Al-dopants could affect the stability of the skeleton, we plot the MSD (mean square displacement) of O (oxygen) and P (phosphorus) of LTP, LATP-0.16 and LATP-0.50 from AIMD simulation under 500 and 900 K, as shown in Fig. S3 in ESI. Comparison of LATP with LTP shows enhanced vibrations of O and P, which allows local relaxation and changes in Li coordination and thus enhances Li-ion conduction.

In summary, we find an ultra-fast Li-ion diffusion within LATP-0.50. From low to high Al-concentration, Li-ion diffusion changes from local oscillation to isolated hopping to superionic flow, faster Li-ion mobility is achieved. However, further optimization towards the Al-concentration is constrained by the cost of computers due to a large number of atoms.

Analysis of Li-ion migration energy profile and electronic structure in LATP

To further understand the high ionic conductivity in LATP-0.50, we calculated the Li-ion migration energy profile using the climbing image nudged elastic band (cNEB) method through

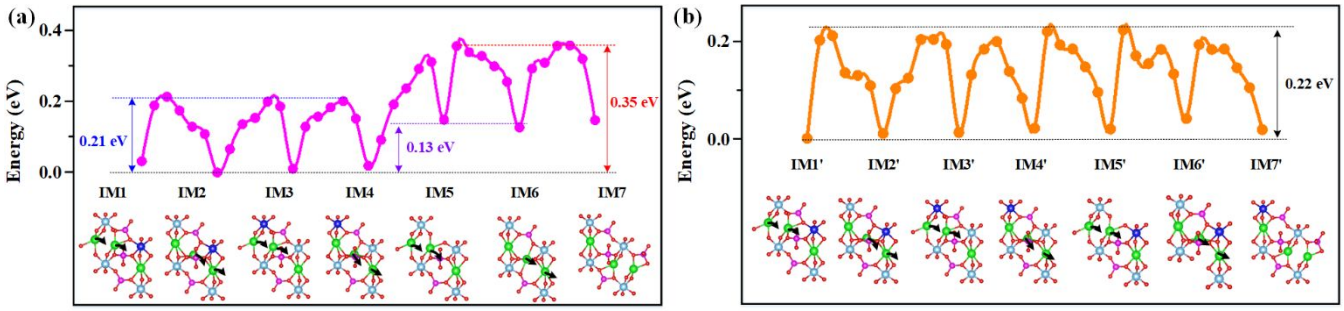

Fig. 5. (a) and (b) Energy profile and schematic drawing of the Li-ions cooperative migration pathway in LATP-0.16 and LATP-0.50. The insets are the schematic drawing of intermediate states along the migration pathway.

two-Li-ions cooperative migration, together with LATP-0.16 as a reference. The results are shown in Fig. 5. The two Li-ions cooperative migration involves a concerted knock-off motion of Li(3)-Li(3) or Li(2)-Li(1) along the diffusion channel. For LATP-0.16 (Fig. 5a), the energy profile of cooperative migration suggests that Li-ion undergoes two stages: IM1 → IM4 and IM4 → IM7. In IM1→ IM4 stage, Li-ion migration occurs near AlO_6-octahedra and the energy change between initial and final states is very small, such as IM1, IM2, IM3, and IM4. In IM4 → IM7 stage, the energy difference between two local energy minima structures (IM4 and IM6) is about 0.13 eV, which increases the energy barrier from 0.21 eV to 0.35 eV. The local energy minima structures near AlO_6 octahedra are more stable than those far away from it, suggesting a trapping effect of Al-dopants[21].

For LATP-0.50, the energy profile of cooperative migration suggests that the energies for all local energy minima structures are uniform and the Li trapping almost vanishes. More importantly, the energy barrier is also uniform and is approximately 0.22 eV, which is lower than that of LATP-0.16. This result is consistent with the AIMD calculations as shown in Fig. 2 and reveals an ultra-fast diffusion process cooperatively.

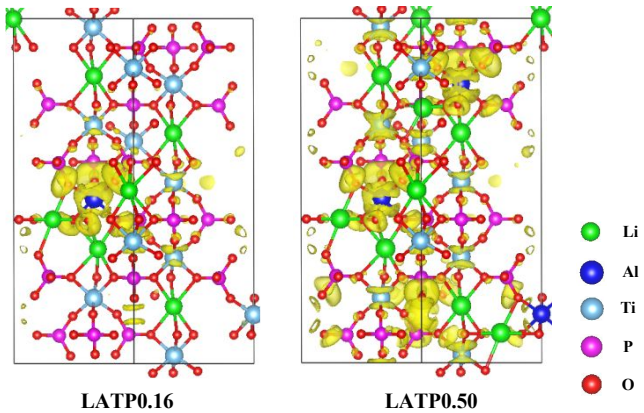

Fig. 6. Charge density differences of LATP-0.16 and LATP-0.50 with respect to LTP and Li. The yellow region represents charge accumulation; the isosurface value is 1×10^{-3} e per $Å^3$.

To understand the electronic structures, Fig. 6 shows the three-dimensional charge density difference by subtracting the electronic charge of the LTP and Li-atoms from LATP. The yellow region represents electron accumulation. It is clear that there are more electrons localized on O-atoms. The higher negative charge on oxygen will lead to larger interaction energies of oxygen toward Li. This finding means that the AlO_6 groups are the polarization centers, which could provide strong interaction between Li and AlO_6. However, in LATP-0.50, the increase of AlO_6 groups delocalizes the effects by the mutual interaction and makes the potential surface more uniform. The Bader charge calculations also suggest that a higher negative charge exists on the O atoms surrounding the Al-dopant, increasing from -1.30 in TiO_6 to -1.50 in AlO_6. Therefore, the trapping effect of AlO_6 leads to interaction between Li and O to be weakened in LATP-0.50, which can enhance the Li-diffusion.

Analysis of cooperative migration mechanism

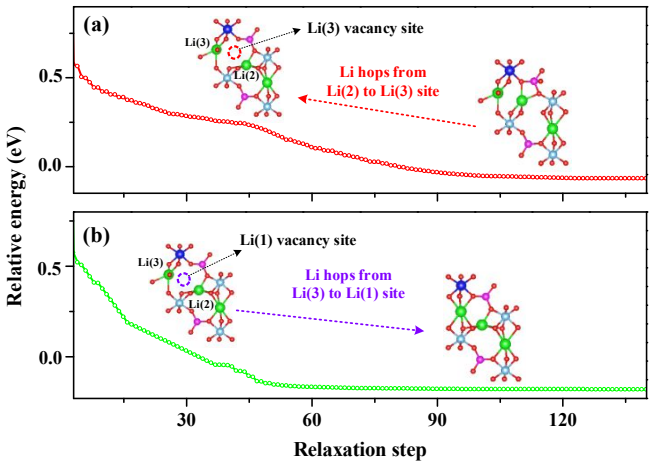

Fig. 7. Li-ion isolated hopping in LATP from DFT energy minimization. (a) Li hops from Li(2) to Li(3) site, and (b) Li hops from

Li(3) to Li(1) site. The corresponding structures highlight the hopping path.

To explain this cooperative migration, we first divide the cooperative migration into two single-Li-ion hopping processes by fixing one of them and relaxing the other one, as shown in Fig. 7. The configuration energy for the single-Li-ion relaxation process in Fig. 7a and 7b, displays opposite trend, in which the single-Li-ion hopping processes need a much higher energy barrier than that of the cooperative migration. This analysis suggests that during the cooperative migration of two Li-ions, the Li-ions located at the high-energy sites migrate downhill, which cancels out a part of the energy barrier felt by other uphill-climbing Li-ions. This finding is in excellent agreement with the recent calculation by Mo et al.[22] for fast Li-ion conductors. In addition, for $Li(2)O_5$ structure, the Li(2) Bader charge change is +0.13 which is higher than that of Li(1) (+0.10) . The higher the Li charge, the lower covalence degree in Li-O bonds. According to that, Li(1) and Li(2) has different potential energy in energy profile of LATP. Therefore, from the energy point, the energy difference between Li(2) and Li(1) result in a cooperative migration.

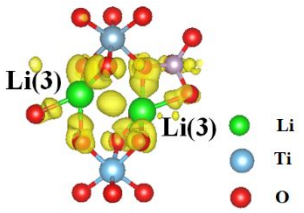

Fig. 8. Electron distribution of $Li(3)O_4$-$Li(3)O_4$ structure with respect to $Ti_2(PO_4)_3$ framework. The yellow region represents charge accumulation; the isosurface value is 1×10^{-3} e per $Å^3$.

Next, by closely inspecting the intermediate states as shown in Fig. 5, we can further attribute the high ionic conductivity of LATP to the oxygen atoms' arrangement, which leads to the $Li(3)O_4$-$Li(3)O_4$ structures with unsymmetrically tetrahedral sites for Li-ions to occupy. Therefore, we calculate the electron distribution of $Li(3)O_4$-$Li(3)O_4$ configuration as shown in Fig. 8. We find there is electron density in the vicinity of two Li-ions, suggesting the interaction between adjacent Li-ions. This charge density could attract two Li-ions causing two Li-ions to pair up. Such two Li-ions suggestion is consistent with the results in Fig. 5 when the Li-ions migrate in pairs, two Li(3)-ions proceeds to the next neighboring Li-sites.

In summary, we identify that the ultra-fast Li-ion diffusion within LATP-0.50 originates from two fundamental reasons. One is the reduced Al-trapping effects for Li-ion hopping which helps to modify the potential energy surface and decreases the Li-ion migration barrier. Another is the interconnection among locally distorted LiO_n-polyhedra ($Li(3)O_4$ or $Li(2)O_6$) within LATP which reduces the distance between consecutive Li-sites. The energy difference of Li(2) and Li(1) and the binding interaction of two Li(3)-ions leads to cooperative migration. The two factors can be transformed each other when Li-ions migrate along the diffusion channel.

Conclusions

In this work, an atomic-level investigation has allowed us to gain valuable insights into the Li-ion cooperative diffusion mechanism in LATP. Three important features are highlighted. i) The highest Li conductivity is observed at the highest considered concentration of Al-dopant, i.e., $Li_{1.5}Al_{0.5}Ti_{1.5}(PO_4)_3$. This opens up the possibility that LATP is among the best in current solid electrolytes with ultra-fast Li-diffusion cooperatively. ii) A high concentration of Al-dopant leads to a smooth energy landscape combining small energy barriers. iii) Li-ion conduction occurs through a cooperative migration mechanism involving concerted knock-off motion of neighboring Li-ions via Li-Li interaction. An important feature is the unique $Li(3)O_4$-$Li(3)O_4$ structure, which allows considerable interaction between Li-ions. The energy difference of Li(2) and Li(1) and the binding interaction of two Li(3)-ions alternately enable the cooperative migration. These findings are believed to be important for the optimization and design of the next generation of inorganic solid-state electrolytes for ASSLBs and warrants further investigation.

Methods

All density functional theory calculations are carried out using the Vienna *ab initio* simulation package (VASP) [38] within the projector augmented wave (PAW) approach[39]. The generalized gradient approximation is adopted in the parameterization of Perdew, Burke, and Ernzerhof (PBE) to describe the exchange-correlation functional with a kinetic energy cut-off of 500 eV.[40,41] A k-mesh (2 × 2 × 1) was generated using the Monkhorst-Pack method to sample the Brillouin zone. All atomic positions and lattice parameters were allowed to relax until the forces on the atoms were less than 0.01 eV/Å. Convergence was finished when the residual forces were below 0.01 eV/Å and the total energy difference was below 10^{-6} eV/atom.

To search for the possible Li-ion migration pathways and the corresponding migration barriers, the climbing image nudged elastic band (cNEB) method was used as implemented in VASP. [42] A chain of five initial images between two local energy minima structures was first set by linear interpolation and then fully relaxed. The Al defect formation energy and phase decomposition energy are calculated and the equations are shown in ESI.

For Li-ion diffusivity calculations, AIMD method employing DFT-based force evaluation with a Verlet algorithm to integrate Newton's equations of motion was performed in VASP software. The NVT (or canonical) ensemble is selected by setting parameters in input file and specifying a Nose-Hoover thermostat. A unit cell containing 136 atoms (16 formula units) and a Γ-point only k-point sampling are chosen for all calculations. The input structure was obtained from the PBE lattice relaxations. The system was equilibrated first under constant pressure of 1 atm and temperature of 500 K for at least 5000-time steps (with a time step of 1 fs). The Li-ion dynamics are performed using the AIMD under the NVT ensemble (at T = 500, 600, 700, 800, 900, and 1000 K) and Nosé thermostat to give a simulation time of 80 ps with time step 1 fs. In certain AIMD cases, the length of time and NVT temperature was set in 30 ps and 900 K to check the jump of Li-ions. The ionic trajectories analyses of AIMD simulations use Python Materials Genomics (pymatgen)[43] and its add-on package pymatgen-diffusion[44].

Conflicts of interest

There are no conflicts to declare.

Acknowledgements

This work was supported by the Soft Science Research Project of Guangdong Province (No. 2017B030301013), Shenzhen Science and Technology Research Grant (ZDSYS201707281026184). Wang was supported by the Assistant Secretary for Energy Efficiency and Renewal Energy of the U.S. Department of Energy under the Battery Materials Research (BMR) program.

Notes and references

1 B. Zhang, R. Tan, L. Yang, J. Zheng, K. Zhang, S. Mo, Z. Lin and F. Pan, *Energy Storage Materials*, 2018, **10**, 139-159.

2 R. Chen, W. Qu, X. Guo, L. Li and F. Wu, *Materials Horizons*, 2016, **3**, 487-516.

3 J. C. Bachman, S. Muy, A. Grimaud, H.-H. Chang, N. Pour, S. F. Lux, O. Paschos, F. Maglia, S. Lupart, P. Lamp, L. Giordano and Y. Shao-Horn, *Chemical Reviews*, 2016, **116**, 140-162.

4 Y. Wang and W.-H. Zhong, *ChemElectroChem*, 2015, **2**, 22-36.

5 S. Ramakumar, L. Satyanarayana, S. V. Manorama and R. Murugan, *Physical Chemistry Chemical Physics*, 2013, **15**, 11327-11338.

6 Y. K. Shin, M. Y. Sengul, A. S. M. Jonayat, W. Lee, E. D. Gomez, C. A. Randall and A. C. T. v. Duin, *Physical Chemistry Chemical Physics*, 2018, **20**, 22134-22147.

7 B. Zhang, L. Yang, L.-W. Wang and F. Pan, *Nano Energy*, 2019, **62**, 844-852.

8 Z. Lin, Z. Liu, N. J. Dudney and C. Liang, *ACS Nano*, 2013, **7**, 2829-2833.

9 C.-W. Ahn, J.-J. Choi, J. Ryu, B.-D. Hahn, J.-W. Kim, W.-H. Yoon, J.-H. Choi, J.-S. Lee and D.-S. Park, *Journal of Power Sources*, 2014, **272**, 554-558.

10 Y. Xiayin, H. Bingxin, Y. Jingyun, P. Gang, H. Zhen, G. Chao, L. Deng and X. Xiaoxiong, *Chinese Physics B*, 2016, **25**, 018802.

11 X. Lu, G. Wu, J. W. Howard, A. Chen, Y. Zhao, L. L. Daemen and Q. Jia, *Chemical Communications*, 2014, **50**, 11520-11522.

12 X. Zhao, Z. Zhang, X. Zhang, B. Tang, Z. Xie and Z. Zhou, *Journal of Materials Chemistry A*, 2018, **6**, 2625-2631.

13 V. Epp, Q. Ma, E.-M. Hammer, F. Tietz and M. Wilkening, *Physical Chemistry Chemical Physics*, 2015, **17**, 32115-32121.

14 M. Kotobuki and M. Koishi, *Ceramics International*, 2013, **39**, 4645-4649.

15 M. Kotobuki and M. Koishi, *Journal of Asian Ceramic Societies*, 2019, **7**, 69-74.

16 B. Davaasuren and F. Tietz, *Solid State Ionics*, 2019, **338**, 144-152.

17 C. Vinod Chandran, S. Pristat, E. Witt, F. Tietz and P. Heitjans, *The Journal of Physical Chemistry C*, 2016, **120**, 8436-8442.

18 S. Breuer, D. Prutsch, Q. Ma, V. Epp, F. Preishuber-Pflügl, F. Tietz and M. Wilkening, *Journal of Materials Chemistry A*, 2015, **3**, 21343-21350.

19 M. Monchak, T. Hupfer, A. Senyshyn, H. Boysen, D. Chernyshov, T. Hansen, K. G. Schell, E. C. Bucharsky, M. J. Hoffmann and H. Ehrenberg, *Inorganic Chemistry*, 2016, **55**, 2941-2945.

20 H. Aono, E. Sugimoto, Y. Sadaoka, N. Imanaka and G. Adachi, *ChemInform*, 1990, **137**, 1023-1027.

21 B. Lang, B. Ziebarth and C. Elsässer, *Chemistry of Materials*, 2015, **27**, 5040-5048.

22 X. He, Y. Zhu and Y. Mo, *Nature Communications*, 2017, **8**, 15893.

23 K. Arbi, S. Mandal, J. M. Rojo and J. Sanz, *Chemistry of Materials*, 2002, **14**, 1091-1097.

24 J. Liu, T. Liu, Y. Pu, M. Guan, Z. Tang, F. Ding, Z. Xu and Y. Li, *RSC Advances*, 2017, **7**, 46545-46552.

25 X. He, Y. Zhu, A. Epstein and Y. Mo, *npj Computational Materials*, 2018, **4**, 18.

26 Z. Deng, Y. Mo and S. P. Ong, *Npg Asia Materials*, 2016, **8**, e254.

27 R. Jalem, Y. Yamamoto, H. Shiiba, M. Nakayama, H. Munakata, T. Kasuga and K. Kanamura, *Chemistry of Materials*, 2013, **25**, 425-430.

28 Y. Mo, S. P. Ong and G. Ceder, *Chemistry of Materials*, 2012, **24**, 15-17.

29 L. O. Hagman, P. Kierkegaard, P. Karvonen, A. I. Virtanen, J. Paasivirta, L. O. Hagman, P. Kierkegaard, P. Karvonen, A. I. Virtanen and J. Paasivirta, *Acta Chemica Scandinavica*, 1968, **22**, 1822-1832.

30 M. Alami, R. Brochu, J. L. Soubeyroux, P. Gravereau, G. Le Flem and P. Hagenmuller, *Journal of Solid State Chemistry*, 1991, **90**, 185-193.

31 D. T. Qui, S. Hamdoune, J. L. Soubeyroux and E. Prince, *Journal of Solid State Chemistry*, 1988, **72**, 309-315.

32 S. Adams, *Acta Crystallographica Section B: Structural Science*, 2001, **57**, 278-287.

33 M. Giarola, A. Sanson, F. Tietz, S. Pristat, E. Dashjav, D. Rettenwander, G. J. Redhammer and G. Mariotto, *The Journal of Physical Chemistry C*, 2017, **121**, 3697-3706.

34 K. Hayamizu and S. Seki, *Physical Chemistry Chemical Physics*, 2017, **19**, 23483-23491.

35 H. Buschmann, J. Dolle, S. Berendts, A. Kuhn, P. Bottke, M. Wilkening, P. Heitjans, A. Senyshyn, H. Ehrenberg, A. Lotnyk, V. Duppel, L. Kienle and J. Janek, *Physical Chemistry Chemical Physics*, 2011, **13**, 19378-19392.

36 S. P. Ong, Y. Mo, W. D. Richards, L. Miara, H. S. Lee and G. Ceder, *Energy & Environmental Science*, 2013, **6**, 148-156.

37 Y. Deng, C. Eames, B. Fleutot, R. David, J.-N. Chotard, E. Suard, C. Masquelier and M. S. Islam, *ACS Applied Materials & Interfaces*, 2017, **9**, 7050-7058.

38 G. Kresse and J. Furthmüller, *Computational Materials Science*, 1996, **6**, 15-50.

39 P. E. Blöchl, *Physical Review B*, 1994, **50**, 17953-17979.

40 G. Kresse and J. Furthmüller, *Physical Review B*, 1996, **54**, 11169-11186.

41 J. P. Perdew, J. A. Chevary, S. H. Vosko, K. A. Jackson, M. R. Pederson, D. J. Singh and C. Fiolhais, *Physical Review B*, 1992, **46**, 6671-6687.

42 G. Henkelman, B. P. Uberuaga and H. Jónsson, *The Journal of Chemical Physics*, 2000, **113**, 9901-9904.

43 S. P. Ong, W. D. Richards, A. Jain, G. Hautier, M. Kocher, S. Cholia, D. Gunter, V. L. Chevrier, K. A. Persson and G. Ceder, *Computational Materials Science*, 2013, **68**, 314-319.

44 Z. Deng, Z. Zhu, I.-H. Chu and S. P. Ong, *Chemistry of Materials*, 2017, **29**, 281-288.

TOC

Bingkai Zhang, Zhan Lin, Huafeng Dong, Lin-Wang Wang, and Feng Pan**

Page 1. – Page 6.

Title: Revealing cooperative Li-ion migration in $Li_{1+x}Al_xTi_{2-x}(PO_4)_3$ solid state electrolyte with high Al doping